Biophysical Journal Volume 109 December 2015 2689–2700

Article

Micromechanical Modeling Study of Mechanical Inhibition of Enzymatic Degradation of Collagen Tissues

Theresa K. Tonge,[1] Jeffrey W. Ruberti,[2] and Thao D. Nguyen[1,*]

[1]Department of Mechanical Engineering, The Johns Hopkins University, Baltimore, Maryland; and [2]Department of Bioengineering, Northeastern University, Boston, Massachusetts

ABSTRACT This study investigates how the collagen fiber structure influences the enzymatic degradation of collagen tissues. We developed a micromechanical model of a fibrous collagen tissue undergoing enzymatic degradation based on two central hypotheses. The collagen fibers are crimped in the undeformed configuration. Enzymatic degradation is an energy activated process and the activation energy is increased by the axial strain energy density of the fiber. We determined the intrinsic degradation rate and characteristic energy for mechanical inhibition from fibril-level degradation experiments and applied the parameters to predict the effect of the crimped fiber structure and fiber properties on the degradation of bovine cornea and pericardium tissues under controlled tension. We then applied the model to examine the effect of the tissue stress state on the rate of tissue degradation and the anisotropic fiber structures that developed from enzymatic degradation.

INTRODUCTION

Collagen is the most abundant protein in the human body and is a key structural component in soft connective tissues, such as skin, cornea, tendon, and blood vessels. Soft connective tissues exhibit a highly organized structure, where stiff collagen fibrils are arranged in a soft matrix of proteoglycans, water, cells, and other non-fibril-forming proteins. The collagen fibrils are organized further into fibers, sheets, and other organ-specific larger-scale structures. The production and organization of the collagen structures can change in response to mechanical stimuli. Mechanical forces and deformation can precipitate growth and remodeling of the tissue structure during physiological processes such as exercising and wound healing, as well as during pathological processes such as fibrosis (1), osteoarthritis (2), and glaucoma (3). Despite the clinical importance of collagen remodeling, the underlying mechanisms of how collagen tissues sense and respond biochemically to mechanical loading are not well understood.

Degradation of the existing collagen structure is an important part of the tissue remodeling process. Mechanical loading can affect the rate of degradation through the actions of fibroblasts, which can sense and respond to forces through the extracellular matrix. Numerous studies have shown that force stimulates the expression of matrix metalloproteinases (MMPs) and tissue inhibitors of MMPs in addition to collagens (4–8). Mechanical stretch also directly influences the rate of enzymatic degradation by altering the collagen mechanochemistry. In an early study, Huang and Yannas (9) stretched a tape of reconstituted collagen fibers prepared from bovine tendon to a fixed extension and allowed the tape to relax to equilibrium. They then subjected the equilibrated, stretched tape to bacterial collagenase and measured the decrease in force with time induced by degradation. They found that the degradation-induced relaxation rate decreased significantly with the applied strain. Mechanical inhibition of collagen degradation has also been observed for tendon collagens (10,11), corneal strips (12,13), and micro-networks of reconstituted collagen type I fibrils (14).

The inhibitory effect of force has also been observed at the fibril level. Flynn et al. (15) performed degradation experiments on single collagen fibrils extracted from bovine sclera and found a significant reduction in the degradation at 0.1% strain and a near cessation of degradation at higher strains. At the molecular level, Camp et al. (16) showed that tensile loads as low as 3 pN decreased by an order of magnitude the enzymatic degradation rate of recombinant human type I collagen monomers by bacterial collagenase. Contrary results have also been reported at the molecular level and tissue level. Adhikari et al. (17) found an eightfold increase in the degradation rate of reconstituted collagen molecules by MMP-1, while Ellsmere et al. (18) showed that strips of bovine pericardium failed at earlier times with increasing loads. However, the data by Ellsmere et al. (18) also showed that the degradation-induced creep rate decreased with increasing applied force in the first hour of the degradation experiment.

The tissue-level studies of Huang and Yannas (9) and later Wyatt et al. (11) also observed that the rate of degradation, as indicated by the rate of degradation-induced stress relaxation, attained a minimum at a stretch that corresponded to the initiation of rapid stiffening in the equilibrium stress-strain

Submitted August 6, 2015, and accepted for publication October 27, 2015.

*Correspondence: vicky.nguyen@jhu.edu

Editor: Fazoil Ataullakhanov.

0006-3495/15/12/2689/12

http://dx.doi.org/10.1016/j.bpj.2015.10.051

response. The initial compliant region of the stress response of collagen tissues is associated with the straightening and recruitment of wavy collagen fibers, while the stiffened region is attributed to the axial stretching of straightened collagen fibers, which transfers the applied force to the collagen molecules. Chang et al. (19) showed in molecular dynamic simulations that the cleavage sites of an unloaded collagen heterotrimer were thermally unfolded from the triple helical structure at body temperature, which may make them vulnerable to MMPs. An applied force causes the triple helical structure to reform at the cleavage sites and may prevent the binding of MMPs.

Previous modeling efforts of the mechanical stabilization of collagen degradation mainly applied phenomenological descriptions of a first-order kinetic process with a strain-dependent degradation rate. These include an exponential dependence of the degradation rate on the fiber strain (20,21), a logistic dependence on fiber strain (22), a bounded evolution equation based on a homeostatic fiber stretch (23), and a sigmoidal decrease with the fiber mechanical strain from a maximum to a minimum at a transition strain (11,24,25). Heck et al. (25) also included the effect of mechanical fiber rupture, and showed that the addition of mechanical rupture was needed to explain the experimental results of Ellsmere et al. (18) that showed faster fiber failure with increased loads.

The goal of this work was to investigate the influence of the fiber-level and tissue-level collagen structure on the mechanical inhibition of enzymatic degradation of collagen tissues. Based on the findings of molecular simulations (19) and single fibril experiments (15), we hypothesized that the rate of enzymatic degradation of collagen materials is inhibited by the axial strain energy density of the collagen fibers. To test this hypothesis, we developed a micromechanical constitutive model for soft tissues based on two central hypotheses. The collagen fibers are initially crimped and respond to an applied force by straightening (bending) before stretching axially. Enzymatic degradation is an energy activated process and the activation energy is increased by the axial strain energy density of the fiber. We fit the parameters for the degradation rate to the single-fibril degradation data of Flynn et al. (15) and fiber mechanical and structural parameters to the equilibrium stress-strain response of the tissues. We applied the model parameters to predict the tissue-level degradation experiments for bovine corneal strips (13) and pericardium strips (18). The model predictions of the degradation-induced creep showed good quantitative agreement with experiments. Finally, we applied the model to study the effect of the crimped fiber structure and properties on the degradation rate as well as alterations in the anisotropic fiber structure with degradation under different biaxial stress states. The findings of this study provide an explanation for the effect of the collagen fiber structure and mechanical loading on the enzymatic degradation process.

MATERIALS AND METHODS

Modeling

In this section, we describe the development of a new, to our knowledge, micromechanical constitutive model for soft collagenous tissue undergoing mechanical loading and enzymatic degradation. The model will be applied in the next section to study the effects of mechanical loading on the rate of enzymatic degradation and anisotropic collagen structure of the tissue. The developments focus on the key assumptions and constitutive relations at the fiber and tissue levels. More detailed developments can be found in the Supporting Material.

Multiscale collagen structure

We begin by assuming that the microstructure of soft collagenous tissues, such as the cornea and pericardium, can be approximated by a two-dimensional (2D) arrangement of long collagen fibers embedded in an incompressible ground substance composed of proteoglycans, other nonfibrillar proteins, and water. The collagen fibers are arranged in all directions in the plane of the tissue, and can exhibit a preferred orientation. The anisotropic collagen structure is described by a 2D probability density distribution of the fiber orientation $\rho(\phi)$ (Fig. 1 *a*). We assume that the fibers are crimped in the undeformed configuration (Fig. 1 *b*) and respond to an applied force by straightening (bending) and stretching axially. For convenience, the fibers are described by a circular cross section with an original radius r_0. Experimental studies of unstrained collagen fibers subjected to bacterial collagenase have shown that degradation proceeds by progressive reduction of the fiber radius (26). Thus, we assume that enzymatic degradation causes r_0 to decrease to r without changing the contour length of the fiber, and define the ratio of the degraded to undegraded radius as $D = r/r_0$. It follows that the original volume of the fiber is related to the degraded volume as $V_f = D^2 V_{f_0}$.

Fiber-level mechanical behavior and degradation kinetics

A number of modeling approaches have been developed to describe the strain-stiffening behavior of collagen fibers. Here, we apply the planar

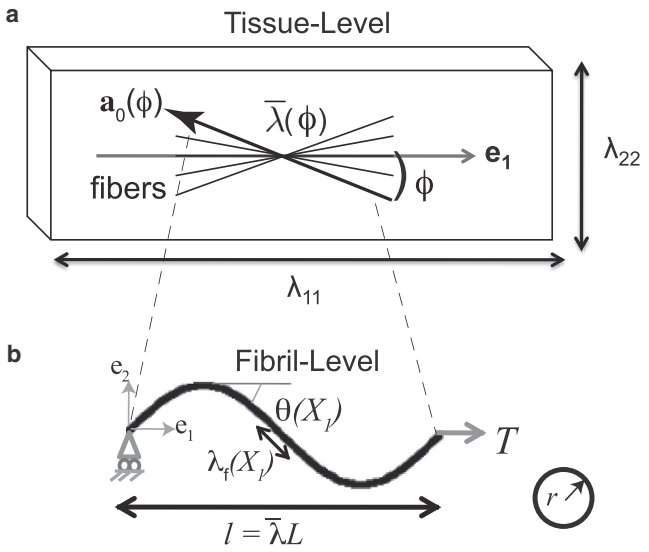

FIGURE 1 Schematic representation of a collagen tissue as a distribution of wavy fibers embedded in an isotropic ground substance. (*a*) The tissue-level deformation imparts an orientation-dependent deformation, $\overline{\lambda}(\phi)$, on each wavy fiber, resulting in an applied fiber force, T. (*b*) The fibril-level stretch is $\lambda_f(X_1)$, and the deformed rotation angle is $\theta(X_1)$.

elastica model of Comninou and Yannas (27) to derive the fiber strain energy density for a crimped collagen fiber. The undeformed configuration of the collagen fiber is represented by a simply supported planar sine wave, $X_2 = a\sin(bX_1)$, where a is the crimp amplitude and has units of length, $L = 2\pi/b$ is the wave length, and the (X_1,X_2) values are the coordinates along the horizontal and vertical directions as illustrated in Fig. 1 *b*. A horizontal force causes the elastica to bend (straighten) and stretch. The deformed configuration is described by the deformed rotation angle $\theta(X_1)$ and axial stretch $\lambda_f(X_1)$. The fiber-level macro-stretch $\overline{\lambda} = l/L$ is defined as the ratio of the deformed to undeformed wave lengths as shown in Fig. 1 *b*.

The following lists the key assumptions of the elastica model (27). 1) The collagen material is linear elastic, described by a Young's modulus, E; and EA and EI denote the axial and bending stiffness of the degrading fiber, respectively, where A is the degraded cross-sectional area and I is the degraded second moment of area. 2) Fibers are allowed to compress by bending. 3) The axial stretch of the fiber is small, thus we can neglect the change in A and I with deformation. 4) The fiber has a thin cross section compared to the length and negligible transverse shear deformation (Euler bending). 5) The undeformed crimp angle $\Theta_0 = ab$ is small, such that the rotation angle of the midline, defined as $\tan\Theta(X_1) = dX_2/dX_1$, can be approximated as $\Theta(X_1) = ab\cos(bX_1)$. With these assumptions, an analytical solution can be derived for the deformed rotation angle, $\theta(X_1)$; fiber micro-stretch, $\lambda_f(X_1)$; and fiber macro-stretch, $\overline{\lambda}$, for an applied tip force T:

$$\theta\left(\overline{X}_1\right) = \frac{D^2\beta}{\alpha(1+\alpha)+D^2\beta}\Theta\left(\overline{X}_1\right), \qquad \Theta\left(\overline{X}_1\right) = \Theta_0\cos\left(2\pi\overline{X}_1\right), \tag{1}$$

$$\lambda_f\left(\overline{X}_1\right) = 1+\alpha\cos\left(\theta\left(\overline{X}_1\right)\right), \tag{2}$$

$$\overline{\lambda} = \int_0^1 \lambda_f\left(\overline{X}_1\right)\frac{\cos\left(\theta\left(\overline{X}_1\right)\right)}{\cos\left(\Theta\left(\overline{X}_1\right)\right)}d\overline{X}_1, \tag{3}$$

where we have introduced the normalized coordinate $\overline{X}_1 = X_1/L$ and nondimensional parameters $\alpha = T/EA$ for the normalized applied force and $\beta = b^2r_0^2/4$ for the slenderness of the wavy beam. We refer the reader to Comninou and Yannas (27) for a detailed derivation of Eqs. 1–3. The combination $E\beta$ describes the flexural stiffness of the beam. The normalized force α is an internal variable that is obtained by solving iteratively the combined Eqs. 1–3 for a given macroscopic fiber stretch $\overline{\lambda}$ (see the Supporting Material).

Assuming small fiber stretch λ_f and small crimp angle Θ_0, the strain energy density of the degraded fiber per unit of degraded volume can be expressed as

$$U_f = \int_0^1 \underbrace{\left[\frac{E\beta D^2}{2}\left(\theta\left(\overline{X}_1\right)-\Theta\left(\overline{X}_1\right)\right)^2\right]}_{U_{\text{bend}}} d\overline{X}_1 + \int_0^1 \underbrace{\left[\frac{E}{2}\left(\lambda_f\left(\overline{X}_1\right)-1\right)^2\right]}_{U_{\text{axial}}} d\overline{X}_1. \tag{4}$$

The first term describes the contribution from straightening and the second term is the contribution from stretching. The formulation in Eq. 4 assumes that differences between the contour length of the deformed and undeformed fiber and the wave length of the undeformed fiber can be neglected. These assumptions are consistent with the solutions for the deformed fiber stretch and rotation angle in Eqs. 1–3 developed by Comninou and Yannas (27). In the Supporting Material, we provide a detailed derivation of the strain energy density in Eq. 4 and estimate the errors associated with the small crimp angle and small fiber strain assumptions.

Collagen degradation kinetics

We developed a zero-order rate equation for the decrease in the fiber radius ratio to model the effects of enzymatic degradation. We chose to decrease the radius based on the experimental observations of Cunningham et al. (26) and Flynn et al. (15). The choice of a zero-order kinetic relation was motivated by enzymatic degradation experiments of both strained and unstrained collagen fibers (28) and collagen gels (28,29) in collagenase showing a constant degradation rate, and is consistent with the zero-order Michaelis-Menten kinetics for an enzyme-mediated reaction in the presence of excess enzyme (11,28). Based on the molecular simulation results of Chang et al. (19) and the experimental observations of Huang and Yannas (9), we assumed that collagen binding and cleavage are energy activated processes, and that the activation energy is increased by the axial strain energy density per unit degraded volume. A simple zero-order rate law that incorporates these assumptions under isothermal conditions is

$$\frac{dD}{dt} = -G_1\exp\left[-\frac{U_{\text{axial}}}{G_2}\right], \tag{5}$$

where U_{axial} is defined in Eq. 4 and $D = r/r_0$ is the ratio of the degraded to undegraded radius of the fiber. The rate law depends on the axial strain energy density per degraded volume rather the axial strain energy density per undegraded volume because the former describes the intrinsic material properties of the fiber. The constant G_1 is the intrinsic degradation rate of the unstrained fiber, and G_2 is the characteristic energy density for mechanical inhibition of the degradation process. By inhibiting the degradation rate with U_{axial} rather than the total U_f, the model allows degradation to proceed only at low stress levels, where fiber elongation proceeds mainly by straightening.

Tissue-level stress relations

We applied the distributed fiber modeling approach to describe the anisotropic hyperelastic behavior at the tissue level. The modeling approach was introduced by Lanir (30) for skin and has been applied to a wide variety of tissues (31–33), including the cornea (34) and pericardium (35). In the model, the collagen fibers and ground substance are assumed to deform affinely with the macroscopic deformation gradient, $\mathbf{F} = \partial\mathbf{x}/\partial\mathbf{X}$, where $\mathbf{X}$ denotes the undeformed coordinates and $\mathbf{x}$ denotes the deformed coordinates of material points. Thus, the macroscopic stretch of a collagen fiber can be evaluated as $\overline{\lambda}(\phi) = (\mathbf{a}_0(\phi)\cdot\mathbf{C}\mathbf{a}_0(\phi))^{1/2}$, where $\mathbf{a}_0(\phi)$ is the unit orientation vector of a fiber along ϕ defined in the reference configuration and $\mathbf{C} = \mathbf{F}^{\mathrm{T}}\mathbf{F}$ is the right Cauchy-Green deformation tensor.

We assume that the strain energy density of the degrading tissue can be defined as the sum of an isotropic contribution from the ground substance and an anisotropic contribution from the collagen fibers undergoing enzymatic degradation, $W = W_{\text{matrix}} + W_{\text{col}}$. For simplicity, the incompressible Neo-Hookean potential is used to describe the isotropic behavior of the ground substance:

$$W_{\text{matrix}} = \frac{\mu}{2}(I_1-3) - \frac{p}{2}(I_3-1). \tag{6}$$

The $I_1 = \text{trace}[\mathbf{C}]$ and $I_3 = \det[\mathbf{C}]$ are the first and third invariants of $\mathbf{C}$, while p enforces the incompressibility constraint, $I_3 = 1$.

For the collagen contribution, we assume that enzymatic degradation causes the collagen volume to decrease without the loss of tissue volume. This assumption applies when the degraded collagen volume is small compared to the original volume. The loss of a significant volume of

collagen would compromise the network structure of the extracellular matrix and cause the surrounding proteoglycans and other nonfibrillar components to dissociate from the tissue, resulting in a loss of tissue volume. From this assumption, the anisotropic component of the tissue-level strain energy density can be determined by integrating the strain energy density of collagen fibers per unit reference volume weighted by the probability density distribution $\rho(\phi)$ over all orientations. The strain energy density per unit reference volume of the fiber can be expressed as $D^2(\phi)U_f$, where U_f is the strain energy density per unit degraded volume defined in Eq. 4. Then, the anisotropic fiber contribution to the tissue strain energy density is given by

$$W_{\text{col}} = \int_{-\pi}^{\pi} U_f\left(\overline{\lambda}(\phi), D(\phi)\right) D^2(\phi)\rho(\phi)d\phi\,. \qquad (7)$$

The $D^2(\phi)\rho(\phi)$ describes the 2D orientation distribution of the remaining collagen volume fraction, while $\int_{-\pi}^{\pi} D^2(\phi)\rho(\phi)d\phi$ denotes the total remaining collagen volume fraction. While the assumption of a 2D fiber structure may be reasonable for the cornea (34), it does not apply in general to all connective tissues. For tissues that have a three-dimensional fiber structure, W_{col} can be formulated as a surface integral over a unit sphere of the fiber strain energy density weighted by an initial three-dimensional distribution function ρ of the fiber orientation, such as the von Mises distribution function (32,36) or the more general Fisher-Bingham distribution (37).

The Cauchy stress can be derived from the strain energy density using the standard hyperelastic definition as

$$\boldsymbol{\sigma} = \mu\mathbf{b} - p\mathbf{I} + \int_{-\pi}^{\pi} \frac{\partial U_f\left(\overline{\lambda}(\phi), D(\phi)\right)}{\partial\overline{\lambda}(\phi)} \frac{1}{\overline{\lambda}(\phi)} \mathbf{F}\mathbf{a}_0(\phi)\otimes\mathbf{F}\mathbf{a}_0(\phi) D^2(\phi)\rho(\phi)d\phi, \qquad (8)$$

where $\mathbf{b} = \mathbf{F}\mathbf{F}^{\mathrm{T}}$ is the left Cauchy-Green deformation tensor and $\mathbf{I}$ is the identity tensor. The derivative of the fiber strain energy density with respect to the macroscopic fiber stretch, $\overline{\lambda}(\phi)$, in Eq. 8 is derived in the Supporting Material.

In summary, enzymatic degradation in the model alters the collagen structure and mechanical behavior at both the tissue and fiber level. At the fiber level, degradation decreases the slenderness ratio β of the collagen fiber by D^2 as shown in Eq. 4. This decreases the bending stiffness and causes the degrading fiber to straighten and creep under constant load. At the tissue level, degradation decreases the tissue stiffness by decreasing the collagen volume fraction, which also produces creep under load.

Determining model parameters from experiments

Table 1 lists the parameters of the constitutive model determined of the cornea and pericardium tissues. For the bovine cornea, we determined the kinetic parameters G_1 and G_2 from the single fibril experiments of Flynn et al. (15) and the fiber mechanical parameters from the equilibrium uniaxial stress response of the bovine corneal strips in Zareian et al. (13). Both studies used the same bacterial collagenase and buffer solutions. Flynn et al. (15) subjected isolated straight bovine scleral fibrils in bacterial collagenase under zero, low (2 pN/monomer), and high (24 pN/monomer) loads. Based on estimations of the number of monomers per fibril and the initial fibril radius, these corresponded to a total force of 0, 46, and 1054 nN for the three cases. The initial diameters for the fibrils were 415, 275, and 225 μm for the zero-, low-, and high-load experiments, respectively. For a straight fibril of initial radius r_0 and degraded radius r subjected to a constant force T, the true stress experienced by the fibrils is $\sigma = T/(\pi {r_0}^2 D^2)$, and the fibril stretch is $\lambda_f = 1 + T/(\pi {r_0}^2 D^2 E)$, assuming small fibril strains. The axial strain energy density defined in Eq. 4 for a straight fibril simplifies to $U_{\text{axial}} = (1/2)T^2/(\pi^2 r_0^4 D^4 E)$. We applied the U_{axial} for a straight fibril to the kinetic relation in Eq. 5 to simulate the degradation experiments using the Young's modulus $E = 0.7$ GPa and initial radius and applied force given by Flynn et al. (15). The intrinsic degradation rate $G_1 = 6.8\text{e}{-4}$ s^{-1} was determined from the slope of the fibril radius plotted as function of time for the zero-load case in the first 1000 s of the degradation experiment. The parameter $G_2 = 7.0\text{e}{-4}$ mJ/mm^3 was fit to the fibril radius measurements in the first 1000 s of the experiments for the 46 nN low-load case. Table 1 lists the parameters from the single-fibril fit, and Fig. 2 compares the model fits with the experimental data of Flynn et al. (15). Also included in the figure is the simulation for the 1054-nN high-load case, which shows near-zero degradation as observed in experiments. For the $G_2 = 7\text{e}{-4}$ mJ/mm^3 obtained from the single-fibril experiment, the degradation rate became effectively zero at 0.3% axial strain.

TABLE 1 Model Parameters

Physical Significance	Definition	Straight Collagen Fibril	Cornea Strip	Pericardium Strip
Unstrained degradation rate	G_1 (s^{-1})	6.8e−4	6.8e−4	1.0e−4
Strain sensitivity parameter	G_2 (mJ/mm^3)	7.0e−4	7.0e−4	7.0e−4
Axial stiffness	E (MPa)	700	50	60
Slenderness ratio	β	—	4.0e−3	0.55e−3
Crimp angle (degrees)	Θ_0	—	29.0	36.0
Matrix shear modulus	μ (MPa)	—	0.026	0.026

To determine the fiber parameters, the Cauchy stress relation in Eq. 8 was applied to solve for the incompressible uniaxial stress response, where for an applied loading σ_{11}, $\sigma_{22} = \sigma_{33} = 0$ and $I_3 = 1$. The Supporting Material provides a derivation of the biaxial stress relations. We assumed an initially isotropic orientation distribution function, $\rho(\phi) = 1/2\pi$, for both the cornea and pericardium. We used $\mu = 26$ kPa for the shear modulus of the isotropic ground substance, which was obtained previously from inflation tests of bovine cornea (38). The remaining three parameters for the fiber modulus E, slenderness ratio β, and crimp angle Θ_0 were chosen to fit the stress-strain data points at the end of the 15-min creep-in period for the three load-levels of the corneal strip experiments of Zareian et al. (13). An optimized fit was not possible given only three data points for the equilibrium stress response. To further constrain the problem, we followed the analysis

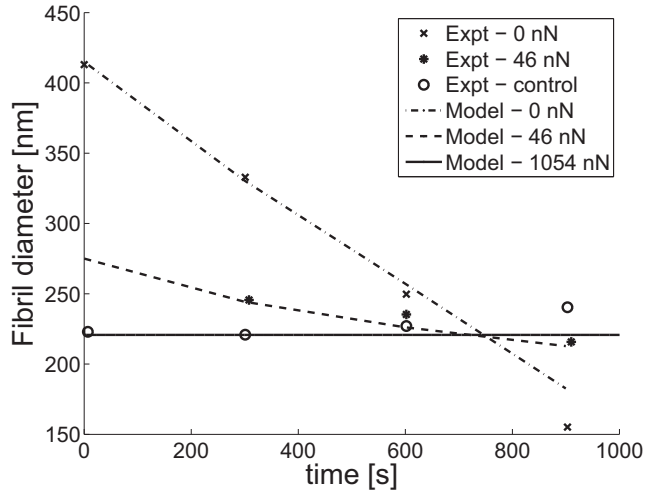

FIGURE 2 Model fit of fiber degradation kinetic parameters to single-fibril degradation data of Flynn et al. (15) for isolated bovine sclera fibrils at different axial loads.

of Zareian et al. (13), which showed that the strain-stiffening behavior of the collagen fibers occurred between the 0.1 and 0.25 N, to select $\Theta_0 = 29°$. The axial stiffness $E = 50$ MPa was chosen to match the slope between 0.25 and 0.5 N points, and the $\beta = 0.004$ was chosen to match the slope between 0.1 and 0.25 N points. We applied the same procedure to fit the elastica parameters to the stress response of the bovine pericardium measured by Ellsmere et al. (18) for applied forces of 0, 10, and 60 g. The results were $\Theta = 36°$, $E =$ MPa, and $\beta = 0.55$ e−3. The crimp angles $\Theta_0 = 29°$ obtained for the cornea and $\Theta_0 = 36°$ for the pericardium produced errors of 6.4 and 9.8%, respectively, for the small angle approximation (27). Table 1 lists the parameters for both tissues, and Fig. 2 compares the model fits to the experimental data.

RESULTS AND DISCUSSION

Predicting tissue degradation from fibril-level degradation kinetic parameters and crimped fiber structure

We applied the constitutive model and parameters in Table 1 to predict the enzymatic degradation experiments of bovine cornea strips of Zareian et al. (13). In the experiments, enzymatic degradation was initiated after a 15 min creep equilibration period by introducing bacterial collagenase, while maintaining a constant axial force. The experiments examined three load levels, $F_t = 0.1$, 0.25, and 0.5 N. The introduction of collagenase caused the tissue to become more compliant and the creep strain rate to increase significantly under constant load. The creep strain was calculated for a duration of 2 h. We simulated the first 6 min of the experiment, where the reaction rate dominates over diffusion. To simulate the degradation experiments, we applied $\sigma_{11} = F_t/A_t$, where A_t is the deformed area of the tissue strip, and $\sigma_{22} = \sigma_{33} = 0$, and solved iteratively the coupled stress relations in Eq. 8 and degradation kinetics relation in Eq. 5 for the stretches λ_1, λ_2, and λ_3 with the incompressibility constraint $I_3 = 1$. The initial tissue cross-sectional area was $A_t^0 = 4.5$ mm^2 (13). Fig. 3 compares the model prediction of the degradation-induced creep strain with the experimental data. The creep rate was determined for the experimental and modeling results by linear regression of the creep strains over the 360 s time period. The results for the three load levels are given in Table 2. The model predictions for the low 0.1 N and middle 0.25 N loads agreed well with the experimental data (13). This is remarkable, given that the parameters for the enzymatic degradation rate of the fiber were determined from fibril-level experiments. Flynn et al. (15) plotted the cleavage rate as a function and an estimated force per monomer for different experiments from the molecular (16), fibril (15), and tissue levels (13) and found similar rates of mechanical stabilization across the three different length scales. The model predicted a significantly lower degradation rate for the high 0.5 N load than experiments. The discrepancy may be caused by mechanical damage of the degrading tissue, which was not included in the model.

We applied the same methods to predict the enzymatic degradation of the bovine pericardium strips of Ellsmere et al. (18). The bovine pericardium strips were subjected to loading to 1, 10, or 60 g within 1.0 s (Fig. 4). The force was held constant, while the strip was exposed to a bacterial collagenase solution, and the degradation-induced creep strain was recorded over a 50 h period. We applied the parameters in Table 1 to predict the uniaxial degradation-induced creep under constant load. We used the same characteristic energy G_2 determined from the single fibril degradation experiments of Flynn et al. (15). However, we had to decrease the intrinsic degradation rate to $G_1 = 1.0 \times 10^{-4}$ s^{-1} to obtain good quantitative agreement with the experimental data. Ellsmere et al. (18) also used *Clostridium histolyticum* collagenase but in a different Ca^+ buffer solution than Zareian et al. (13). They also used a different collagenase concentration and exposure time, which explains why the intrinsic degradation rate G_1 was different between the two experiments.

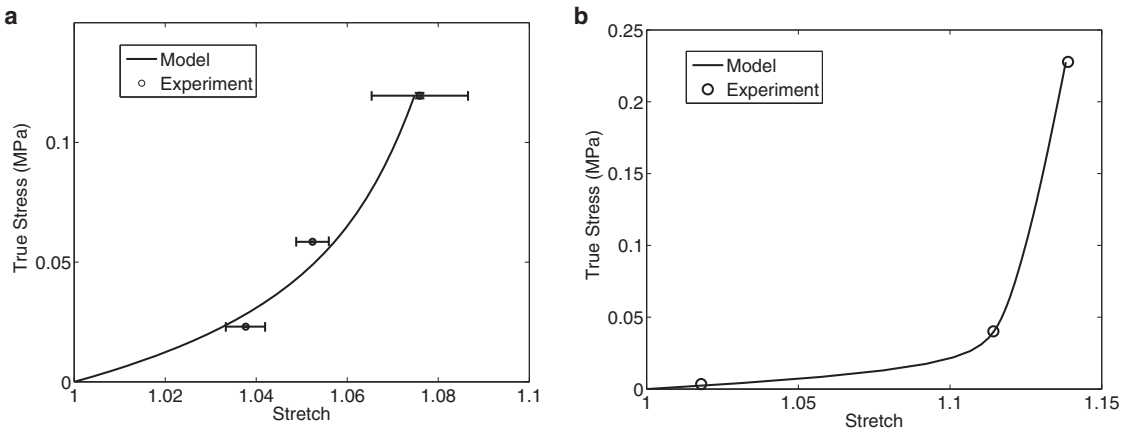

FIGURE 3 Model fit of elastica parameters to the equilibrium uniaxial stress response of (*a*) cornea strips experiments (13) and (*b*) bovine pericardium (18). The model parameters for both tissues are listed in Table 1.

TABLE 2 Creep Rates for the Bovine Cornea Experimental Data and Model Prediction

Force (N)	Engineering Stress (kPa)	Experimental Creep Rate (s^{-1})	Model Creep Rate (s^{-1})
0.1	22.2	7.02e−5 ± 9.9e−7	6.64e−5
0.25	55.6	3.81e−5 ± 6.1e−7	3.31e−5
0.5	111.1	4.90e−5 ± 0.2e−6	1.10e−5

Reported by Zareian et al. (13).

TABLE 3 Creep Rates for Bovine Pericardium Experimental Data and Model Prediction

Force (g)	Engineering Stress (kPa)	Experimental Creep Rate (s^{-1})	Model Creep Rate (s^{-1})
1	3.4	4.25e−6	4.12e−6
10	36	1.70e−6	1.95e−6
60	200	1.39e−6	2.82e−7

Reported by Ellsmere et al. (18).

The creep rate for first 2000 s was determined for the three different load levels using linear regression and shown in Table 3. Fig. 5 plots the creep strain comparing simulation and experiments. The results for both the low 1 g and middle 10 g load agreed well with experiments. For the high 60 g load, the model creep rate was significantly lower than the experimentally measured value. As with the data of Zareian et al. (13), we speculate that the higher load induced mechanical damage, which was not included in the model (25).

An important outcome of the modeling study was that we were able to use the same kinetic parameters G_1 and G_2 to describe the degradation of the single fibril and corneal strip. The difference in the degradation rates of the two different collagen structures at different length scales was captured by the incorporating descriptions of the distributed and crimped structure of the collagen fibers, which were determined from the equilibrium stress response. In addition, we were able to apply the same characteristic $G_2 = 7.0\text{e}{-4}$ mJ/mm^3 for mechanical inhibition to describe the degradation of the cornea and pericardium strips, which have different collagen fiber structures and exhibit very different stress-strain behaviors as shown in Fig. 3. The degradation-induced creep rate was 20 times lower in the experiments of Ellsmere et al. (18) for the pericardium compared to Zareian et al. (13) for the cornea. The ratio of the middle to low loads were also different between the two experiments, but both showed that the degradation-induced creep rate decreased by one-half from the low- to middle load levels. We were able to reproduce the differences in the degradation-induced creep rate for these tissues by incorporating the differences in their fiber structure and tuning the intrinsic degradation rate G_1 for the pericardium data.

Fiber crimp structure significantly influences the degradation rate

We performed a parameter study to investigate the effects of the fiber structure and kinetic parameters on the degradation-induced creep of collagen tissues. We used the parameters in Table 1 for the corneal strip as the baseline and varied each parameter one-by-one between 0.1 and 3.0 times the baseline. This range included the values of the parameters determined for the pericardium strips. We varied the Young's modulus E while keeping the bending stiffness $E\beta$ constant to examine the sole effect of the axial stiffness. Fig. 6 a plots the degradation-induced creep rate at the middle load $F_t = 0.25$ N from the study by Zareian et al. (13), normalized by the creep rate obtained for the baseline

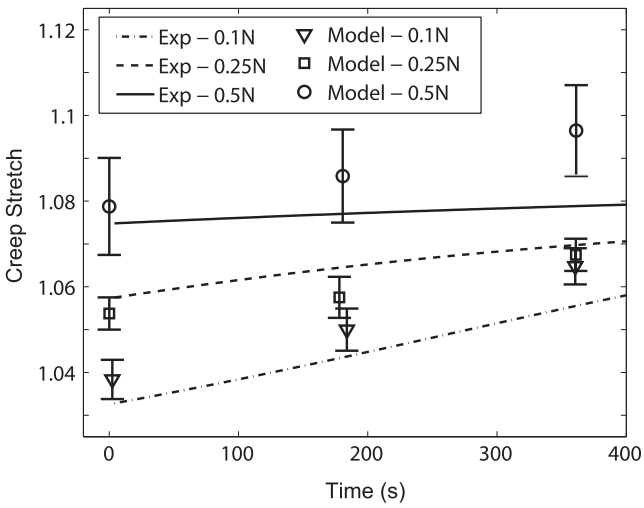

FIGURE 4 Prediction of enzymatic degradation experiments of bovine cornea strip under load, comparing the model prediction and experimental data of Zareian et al. (13).

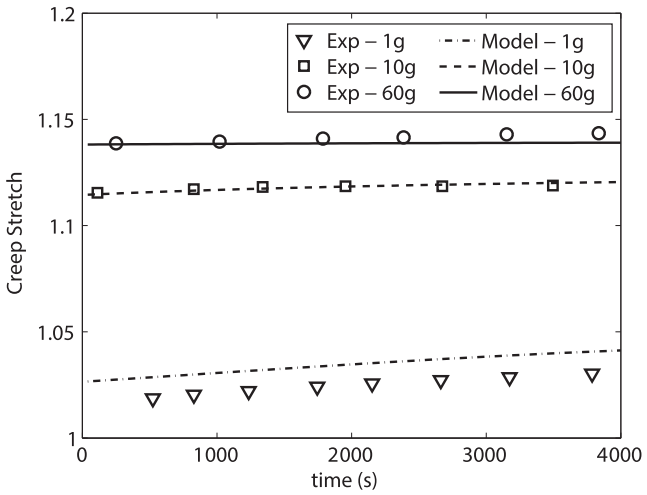

FIGURE 5 Prediction of enzymatic degradation experiments of bovine cornea strip under load, comparing the model prediction and experimental data of Ellsmere et al. (18).

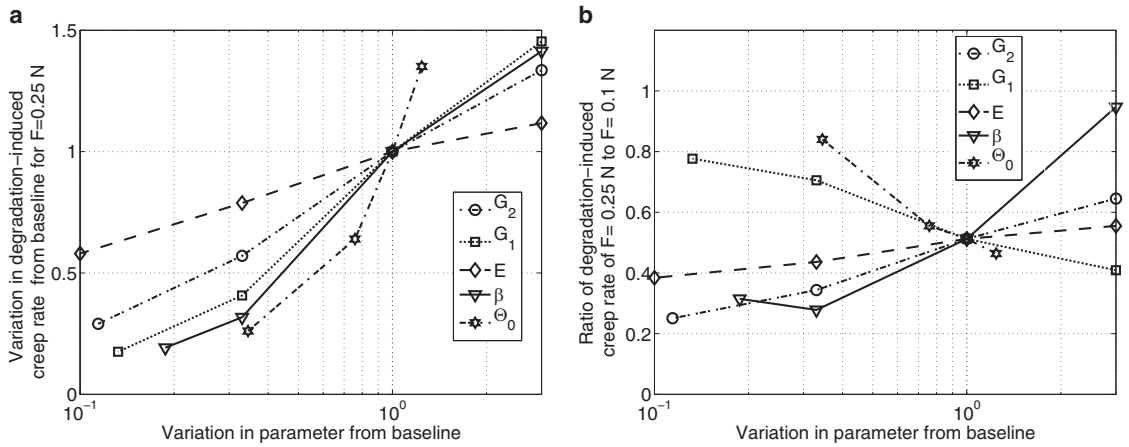

FIGURE 6 Effects of the fiber structure and kinetic parameters on degradation-induced creep rate. The parameters for the bovine cornea in Table 1 were used as the baseline for the parameter study. (*a*) Creep rate for applied $F_t = 0.25\ N$ normalized by baseline in Table 2. (*b*) Ratio of creep rate for $F_t = 0.1\ N$ to $F_t = 0.25\ N$.

parameters. As expected, the degradation-induced creep rate decreased with the intrinsic degradation rate G_1 and mechanical energy threshold G_2. However, the mechanical parameters describing the fiber crimp structure, axial stiffness, and bending stiffness also had a significant effect. Fibers with more compliant axial stiffness, smaller bending stiffness (smaller β), and smaller crimp angle experienced slower degradation rates. More compliant fibers and those with less crimp straighten at lower loads thus they experience mechanical inhibition at lower loads. Fig. 5 *b* plots the ratio of the creep rates obtained for the middle load $F_t = 0.25\ N$ and the low load $F_t = 0.1\ N$. A smaller ratio indicated a larger mechanical inhibition effect. We obtained a smaller ratio of the creep rates for a larger intrinsic degradation rate G_1 and for fibers with larger crimp angles Θ_0 and lower bending stiffness. A larger mechanical inhibition effect was obtained for more flexible fibers because these straighten under lower loads. A larger G_1 caused a larger decrease in the slenderness ratio of the degrading fiber, which made the fiber more compliant in bending and produced greater mechanical inhibition at the same load. Interestingly, the axial modulus E had the least effect on mechanical inhibition. The energy threshold G_2 for mechanical inhibition was small, thus mechanical inhibition was obtained for very small fiber axial strains. The degradation rate became effectively zero at 0.3% axial strain, which was an order of magnitude smaller than the strain at which the fibers straighten. As a result, the effect of mechanical inhibition was more sensitive to the fiber-crimp angle Θ_0 and slenderness ratio β than to G_2. A larger effect would have been obtained if we had varied G_2 such that the axial strain threshold for mechanical inhibition became larger than the straightening strain of the fiber. This would cause the tissue degradation process to be more sensitive to the kinetics parameters rather than the fiber structure. These findings suggest that the fiber structure may provide a means by which collagenous tissues influence the force level that stimulate remodeling.

The rate of tissue degradation depends on the stress state

We applied the constitutive model and the parameters for bovine cornea in Table 1 to investigate the effects of the stress state on the tissue degradation. Recall that the undegraded collagen structure of the tissue was assumed to be isotropic, with the initial fiber volume fraction distributed randomly in all orientations. We first assessed the effect of different stress levels on the total fiber volume fraction. Fig. 7 plots the remaining fiber volume fraction, defined as $(1/2\pi)\int_{-\pi}^{\pi} D(\phi)^2 d\phi$, over 4000 s, comparing constant uniaxial or equibiaxial stress loading ranging from 10 to 90 kPa. Uniaxial simulations exhibited rapid degradation, which abruptly decreased after 1500 s, although the rate of fiber mass loss remained finite for all applied stresses up to 4000 s. Higher stress resulted in a higher remaining fiber volume fraction, and complete degradation of the fibers was not achieved for any stress level. In contrast, simulations of equibiaxial loading exhibited complete degradation for lower applied stresses. Moreover, the applied stress had a larger effect on the degradation rate. For example, the fiber mass loss between 40 and 90 kPa in the first 500 s decreased by 14% for uniaxial tension compared to 34% for biaxial tension.

To understand these results, we plot the distribution of the fiber volume fraction in Fig. 8 at 400, 800, 1500, and 4000 s for the 40 kPa uniaxial and equibiaxial simulations. Under uniaxial loading (at $\phi = 0°$), off-axis fibers were quickly degraded, while load-bearing fibers were preserved, which was consistent with experimental observations of Ruberti and Hallab (12). Tissues subjected to equibiaxial loading at $\phi = 0°$ and 90° remained isotropic as all fibers degraded

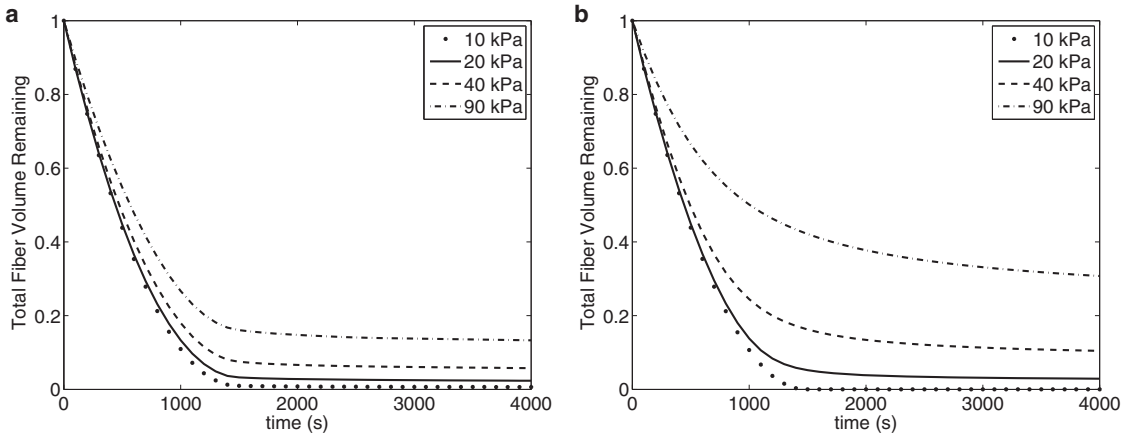

FIGURE 7 The fraction of fiber mass remaining with time, as degradation proceeds for differing levels of (*a*) uniaxial stress and (*b*) equibiaxial stress.

at the same rate. The sudden decrease in degradation rate at 1500 s for uniaxial loading occurred when the unloaded fibers were nearly completely degraded, leaving only the loaded fibers. Because unstrained fibers degraded at the same rate, this transition occurred at approximately the same time for all stress levels. In contrast, for the biaxial case, all fibers were loaded equally and degraded uniformly, at a rate determined by the fiber stretch. As the fibers degraded, the stretch on individual fibers increased under constant stress, slowing degradation. For a very low equibiaxial stress, the fibers degraded completely.

Enzymatic degradation induces collagen anisotropy depending on the tissue stress state

While uniaxial loading can lead to strongly anisotropic fiber structures, many tissues in the body exhibit fiber structures of varying degrees of anisotropy. We next explored the effect of a nonequal biaxial stress state on the degraded fiber mass distribution. We quantified the degree of fiber alignment by computing the ratio of the anisotropic component of the fiber distribution function $D^2(\phi)\rho(\phi)$, above an isotropic baseline, to the total fiber volume fraction (39). The uniaxial stress state described previously resulted in a completely anisotropic fiber structure with no isotropic component (degree of fiber alignment = 1), while the equibiaxial stress state maintained a fully isotropic structure (degree of fiber alignment = 0). Fig. 9 plots the degree of fiber alignment resulting from varying the ratio of σ_{22}/σ_{11} from 0 (uniaxial) to 1 (biaxial) for $\sigma_{11} = 40$ kPa. Below $\sigma_{22}/\sigma_{11} = 0.25$, the tissue became fully anisotropic as off-axis fibers were not strained sufficiently to halt degradation, given the fiber parameters for bovine cornea in Table 1. The anisotropic ratio decreased linearly with the biaxial stress ratio for $\sigma_{22}/\sigma_{11} > 0.25$. Small changes in the biaxial stress state can lead to large changes in the anisotropy of the fiber structure induced by enzymatic degradation. For example, a biaxial stress ratio of 0.625, which was within the range of

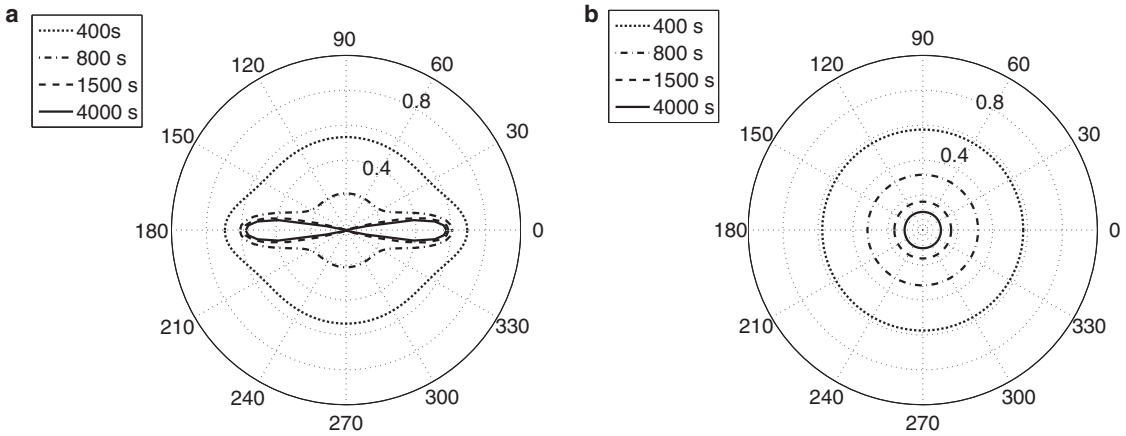

FIGURE 8 Polar plot of the fiber mass distribution after 800, 1500, and 4000 s of degradation for 40 kPa constant stress applied (*a*) uniaxially, at $\phi = 0°$, and (*b*) equibiaxially, at $\phi = 0°$ and 90°.

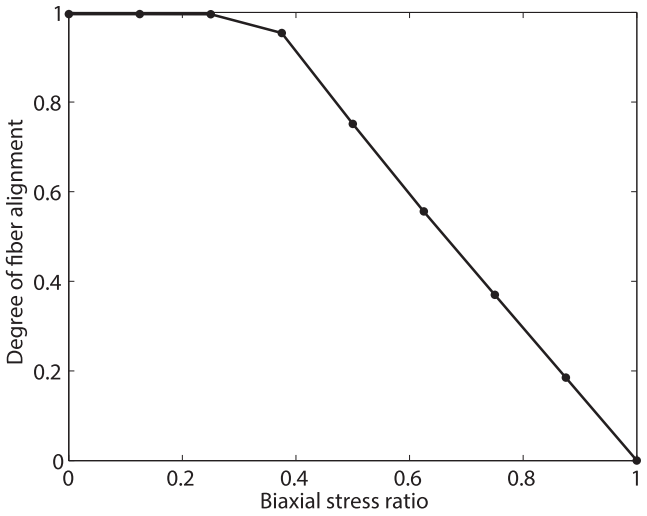

FIGURE 9 Anisotropy ratio for different biaxial stress ratios of σ_{22}/σ_{11} for $\sigma_{11} = 40$ kPa. For $\sigma_{22}/\sigma_{11} < 0.25$, all off-axis fibers are fully degraded, resulting in a completely anisotropic structure (degree of fiber alignment = 1).

stress ratios measured in inflation testing of human sclera (40), produced an anisotropic ratio of 0.56, which was within the range of degree of fiber alignment reported by Pijanka et al. (39) and Coudrillier et al. (41,42) for the human sclera. The results shows that mechanical stabilization of collagen degradation may play a key role in the remodeling of the collagen anisotropy along the directions of the maximum principal stress and the degree of fiber alignment with the biaxial stress ratio.

CONCLUSIONS

We developed a micro-mechanical model for an anisotropic collagen tissue with an initial crimped fiber structure to investigate the microstructural origins of the mechanical inhibition of enzymatic degradation of collagen tissues. The collagen fibers were modeled as wavy beams distributed in all orientations in the plane of the tissue. We applied a simple zero-order kinetic relation with an energy-activated degradation rate for enzymatic degradation of a collagen fiber. The degradation rate was inhibited by the axial strain energy density of the fiber, which increased the activation energy for the degradation reaction. We fit the two kinetic parameters of the degradation rate law to the fibril-level degradation experiments of Flynn et al. (15), which subjected isolated fibrils from bovine sclera to uniaxial loading. The remaining parameters for the fiber stress response were fit to the equilibrium stress-strain response of tissue strips under uniaxial tension. We applied the model to predict the tissue-level degradation experiments of Zareian et al. (13) for bovine corneal strips and Ellsmere et al. (18) for bovine pericardium strips under uniaxial tension. The results showed excellent quantitative agreement of the degradation-induced creep rate. The following is a list of the major findings of this work.

1) We were able to explain the correspondence between the threshold strain for mechanical inhibition of enzymatic degradation and the transition strain of the strain-stiffening stress response by modeling the crimped fiber structure, which allows the fiber to bend and stretch in response to an applied load, and the degradation as an energy-activated process inhibited by the axial strain energy of the collagen fiber. Thus, crimped fibers are degraded at an intrinsic degradation rate, while straightened fibers are protected from degradation.
2) We determined the intrinsic degradation rate and characteristic energy for mechanical inhibition from degradation experiments of an uncrimped collagen fibril. The result for the characteristic energy for mechanical inhibition produced a near-zero degradation rate for axial strains larger than 0.3%. This was significantly smaller than the strain at which the collagen fibers of the cornea and pericardium straighten. Thus, the strain at which mechanical inhibition was observed at the tissue level was determined primarily by the fiber crimp.
3) Results of the parameter study suggest that the effect of mechanical inhibition is strongly dependent on the fiber crimp and the fiber bending stiffness. Fibers that are stiff in bending and with large initial crimp angles straighten at larger mechanical loads. Thus, for the same stress levels, less crimped and more slender fibers are more resistant to enzymatic degradation.
4) For tissues composed of collagen fibers arranged in all orientations, the degradation rate depends on the state of biaxial stress and was more sensitive to the stress level for equibiaxial tension than uniaxial tension. For uniaxial tension, the degradation reduces dramatically with stretch but does not halt entirely, because fibers oriented close to the loading direction continue to slowly degrade. This was observed in the tissue-level experiments of Wyatt et al. (11).
5) Mechanical inhibition of enzymatic degradation under constant load leads to a remodeling of the anisotropy of the fiber structure along the principal stress direction and a remodeling of the degree of fiber alignment with the biaxial stress ratio.

We had a number of limitations to our modeling approach. We did not model the difference between the fibril and fiber collagen structures and the interaction between fibers. In the cornea, collagen fibrils are arranged in parallel into lamellae, referred to as fibers, and the fibers are stacked in different orientations to form the corneal stroma. Incorporating the structural organization of fibrils into fibers and the interaction between fibers through cross links may change the predicted degradation rate for a tissue. It has been speculated that fibrils arranged in fibers experience strain shielding, which causes the fibrils to be degraded even at large tissue stretch. Although we did not consider these effects, the model was able to apply the degradation

rates measured at the fibril level to predict tissue-level degradation rates at short times.

We assumed that all fibers exhibit the same crimp angle and radius, but most tissues likely exhibit a distribution of crimp angles and radii, which would cause some fibers to degrade more quickly than others. The increased stress on the slower degrading fibers may cause inhibition at lower tissue stretch. We did not take into account changes in the tissue volume induced by collagen degradation (i.e., negative growth), leaving this for future studies. Finally, we did not model the effect of diffusion and mechanical damage on the fiber-level and tissue-level creep rates. This limited the applicability of the model to the first 6 min of the experiments of Zareian et al. (13), where, according to our scaling analysis, the creep rate can be ascribed primarily to the reaction-associated degradation effects of the enzyme. At longer times, the process would be retarded by the diffusion distance into the tissue. Moreover, the tissue experienced negligible mechanical damage during this initial period. Extending the predictive ability of the model to longer times and higher stress levels would require a more comprehensive treatment of the coupled deformation-reaction-diffusion process, interaction between fibers, nonuniformity of the fiber structure, and mechanical damage, which is beyond the scope of this work.

We fit the elastica parameters for the collagen fibers to uniaxial tensile experiments of tissue strips after a 15-min creep equilibration period. The resulting parameters were more compliant than measured in previous in vitro inflation tests of bovine cornea (38,43). The parameters produced an initial crimp angle of 29°, which was significantly larger than measured by histology for rabbit cornea (44). The slenderness ratio, $\beta = 0.004$, was also smaller than computed based on the histological measurements for the rabbit cornea. Additionally, only three stress levels were available to fit three mechanical parameters. To limit the potential parameter space, we followed the force-per-monomer calculations of Zareian et al. (13), indicating that the straightening transition occurred between the medium (0.25 N) and high (0.5 N) force levels. This fixed the crimp angle and the remaining two parameters were manually fit to the toe and linear region of the equilibrium stress-strain curve. More data is needed to ensure an optimized parameter set. In the parameter study, we investigated the effect of the fiber structure and kinetic parameters by varying the parameters one-by-one and evaluating the effect on the degradation-induced creep rate of the cornea strip under moderate loading and the effect of mechanical inhibition of the high loading on the creep rate. While the results show that that the structural parameters have a significant effect on the tissue degradation rate and mechanical inhibition of the degradation rate, a multifactorial study design is needed to investigate the sensitivity of the model to parameters that may co-vary (e.g., Johnson et al. (45)).

Finally, the model does not connect to the molecular scale, and the molecular mechanisms underlying the mechanical stabilization of enzymatic degradation of collagen fibrils remain unclear and controversial (46). Mechanical stabilization has been observed at the molecular level by Camp et al. (16). Chang et al. (19) performed molecular dynamics simulation of heterotrimer and homotrimer collagen molecules and found that tensile forces caused structural changes in the cleavage sites of a collagen heterotrimer that may prevent MMPs from binding and cleaving the molecule. Molecular-level degradation experiments have also produced the contrary result, that mechanical strain increases the rate of degradation of a heterotrimeric collagen molecule (17) by matrix metalloproteinases. However, the experimental study by Sarkar et al. (47) suggested that the degradation mechanism of collagen fibrils is different from that of a collagen molecule. The authors tracked the motion of fluorescently labeled MMP1 on rat tail tendon fibrils, and found that MMP1 spends a significant amount of time in a class-II pause state at periodic intervals along the collagen fibril. A small fraction of the pause states results in the initiation of cleavage. The authors postulated that the periodically arranged pause sites correspond to local melting of the fibril that expose the cleavage sites of the molecules. Deformation that straightens and stretches the collagen fibril may change the structure and/or affinity of the pause sites, which would dramatically alter the susceptibility of the fibril to degradation.

SUPPORTING MATERIAL

Supporting Materials and Methods, one figure, and two tables are available at http://www.biophysj.org/biophysj/supplemental/S0006-3495(15)01161-3.

AUTHOR CONTRIBUTIONS

T.K.T. primarily performed the research, wrote the article, and significantly contributed to the model development and research design; J.W.R. contributed to the research design (particularly the application of the experimental data to determine the model parameters and validate the model predictions) and participated in the initial drafting and revising of the article; and T.D.N. significantly contributed to the model development, research design, and initial drafting and revising of the article.

ACKNOWLEDGMENTS

This work was funded by National Science Foundation CAREER Award No. 1253453 (to T.D.N.) and Public Health Service Research Grants NEI-R01EY015500 (to J.W.R.) and R01EYEI021500 (to T.D.N.).

REFERENCES

1. Jalil, J. E., C. W. Doering, …, K. T. Weber. 1989. Fibrillar collagen and myocardial stiffness in the intact hypertrophied rat left ventricle. *Circ. Res.* 64:1041–1050.

2. Sandell, L. J., and T. Aigner. 2001. Articular cartilage and changes in arthritis. An introduction: cell biology of osteoarthritis. *Arthritis Res.* 3:107–113.
3. Quigley, H. A., M. E. Dorman-Pease, and A. E. Brown. 1991. Quantitative study of collagen and elastin of the optic nerve head and sclera in human and experimental monkey glaucoma. *Curr. Eye Res.* 10:877–888.
4. Parsons, M., E. Kessler, …, J. E. Bishop. 1999. Mechanical load enhances procollagen processing in dermal fibroblasts by regulating levels of procollagen C-proteinase. *Exp. Cell Res.* 252:319–331.
5. Prajapati, R. T., B. Chavally-Mis, …, R. A. Brown. 2000. Mechanical loading regulates protease production by fibroblasts in three-dimensional collagen substrates. *Wound Repair Regen.* 8:226–237.
6. Mudera, V. C., R. Pleass, …, R. A. Brown. 2000. Molecular responses of human dermal fibroblasts to dual cues: contact guidance and mechanical load. *Cell Motil. Cytoskeleton.* 45:1–9.
7. Blain, E. J., S. J. Gilbert, …, V. C. Duance. 2001. Up-regulation of matrix metalloproteinase expression and activation following cyclical compressive loading of articular cartilage in vitro. *Arch. Biochem. Biophys.* 396:49–55.
8. Koskinen, S. O. A., K. M. Heinemeier, …, M. Kjaer. 2004. Physical exercise can influence local levels of matrix metalloproteinases and their inhibitors in tendon-related connective tissue. *J. Appl. Physiol.* 96:861–864.
9. Huang, C., and I. V. Yannas. 1977. Mechanochemical studies of enzymatic degradation of insoluble collagen fibers. *J. Biomed. Mater. Res.* 11:137–154.
10. Nabeshima, Y., E. S. Grood, …, J. H. Herman. 1996. Uniaxial tension inhibits tendon collagen degradation by collagenase in vitro. *J. Orthop. Res.* 14:123–130.
11. Wyatt, K. E.-K., J. W. Bourne, and P. A. Torzilli. 2009. Deformation-dependent enzyme mechanokinetic cleavage of type I collagen. *J. Biomech. Eng.* 131:051004.
12. Ruberti, J. W., and N. J. Hallab. 2005. Strain-controlled enzymatic cleavage of collagen in loaded matrix. *Biochem. Biophys. Res. Commun.* 336:483–489.
13. Zareian, R., K. P. Church, …, J. W. Ruberti. 2010. Probing collagen/enzyme mechanochemistry in native tissue with dynamic, enzyme-induced creep. *Langmuir.* 26:9917–9926.
14. Bhole, A. P., B. P. Flynn, …, J. W. Ruberti. 2009. Mechanical strain enhances survivability of collagen micronetworks in the presence of collagenase: implications for load-bearing matrix growth and stability. *Philos. Trans. A. Math. Phys. Eng. Sci.* 367:3339–3362.
15. Flynn, B. P., G. E. Tilburey, and J. W. Ruberti. 2013. Highly sensitive single-fibril erosion assay demonstrates mechanochemical switch in native collagen fibrils. *Biomech. Model. Mechanobiol.* 12:291–300.
16. Camp, R. J., M. Liles, …, J. W. Ruberti. 2011. Molecular mechanochemistry: low force switch slows enzymatic cleavage of human type I collagen monomer. *J. Am. Chem. Soc.* 133:4073–4078.
17. Adhikari, A. S., E. Glassey, and A. R. Dunn. 2012. Conformational dynamics accompanying the proteolytic degradation of trimeric collagen I by collagenases. *J. Am. Chem. Soc.* 134:13259–13265.
18. Ellsmere, J. C., R. A. Khanna, and J. M. Lee. 1999. Mechanical loading of bovine pericardium accelerates enzymatic degradation. *Biomaterials.* 20:1143–1150.
19. Chang, S.-W., B. P. Flynn, …, M. J. Buehler. 2012. Molecular mechanism of force induced stabilization of collagen against enzymatic breakdown. *Biomaterials.* 33:3852–3859.
20. Hadi, M. F., E. A. Sander, …, V. H. Barocas. 2012. Simulated remodeling of loaded collagen networks via strain-dependent enzymatic degradation and constant-rate fiber growth. *Mech. Mater.* 44:72–82.
21. Demirkoparan, H., T. J. Pence, and A. Wineman. 2013. Chemomechanics and homeostasis in active strain stabilized hyperelastic fibrous microstructures. *Int. J. Non-linear Mech.* 56:86–93.
22. Barocas, V. H., K. D. Dorfman, and Y. Segal. 2012. A model of strain-dependent glomerular basement membrane maintenance and its potential ramifications in health and disease. *J. Biomech. Eng.* 134:081006.
23. Grytz, R., I. A. Sigal, …, J. C. Downs. 2012. Lamina cribrosa thickening in early glaucoma predicted by a microstructure motivated growth and remodeling approach. *Mech. Mater.* 44:99–109.
24. Loerakker, S., C. Obbink-Huizer, and F. P. T. Baaijens. 2014. A physically motivated constitutive model for cell-mediated compaction and collagen remodeling in soft tissues. *Biomech. Model. Mechanobiol.* 13:985–1001.
25. Heck, T. A., W. Wilson, …, C. C. van Donkelaar. 2015. A tissue adaptation model based on strain-dependent collagen degradation and contact-guided cell traction. *J. Biomech.* 48:823–831.
26. Cunningham, K. D., F. Musani, …, C. B. Frank. 1999. Collagenase degradation decreases collagen fibril diameters–an in vitro study of the rabbit medial collateral ligament. *Connect. Tissue Res.* 40:67–74.
27. Comninou, M., and I. V. I. Yannas. 1976. Dependence of stress-strain nonlinearity of connective tissues on the geometry of collagen fibers. *J. Biomech.* 9:427–433.
28. Tzafriri, A. R., M. Bercovier, and H. Parnas. 2002. Reaction diffusion model of the enzymatic erosion of insoluble fibrillar matrices. *Biophys. J.* 83:776–793.
29. Welgus, H. G., J. J. Jeffrey, …, A. Z. Eisen. 1980. Characteristics of the action of human skin fibroblast collagenase on fibrillar collagen. *J. Biol. Chem.* 255:6806–6813.
30. Lanir, Y. 1979. A structural theory for the homogeneous biaxial stress-strain relationships in flat collagenous tissues. *J. Biomech.* 12:423–436.
31. Billiar, K. L., and M. S. Sacks. 2000. Biaxial mechanical properties of the native and glutaraldehyde-treated aortic valve cusp: part II—a structural constitutive model. *J. Biomech. Eng.* 122:327–335.
32. Tonge, T. K., L. M. Voo, and T. D. Nguyen. 2013. Full-field bulge test for planar anisotropic tissues: Part II—a thin shell method for determining material parameters and comparison of two distributed fiber modeling approaches. *Acta Biomater.* 9:5926–5942.
33. Coudrillier, B., C. Boote, …, T. D. Nguyen. 2013. Scleral anisotropy and its effects on the mechanical response of the optic nerve head. *Biomech. Model. Mechanobiol.* 12:941–963.
34. Nguyen, T. D., R. E. Jones, and B. L. Boyce. 2008. A nonlinear anisotropic viscoelastic model for the tensile behavior of the corneal stroma. *J. Biomech. Eng.* 130:041020.
35. Sacks, M. S. 2003. Incorporation of experimentally derived fiber orientation into a structural constitutive model for planar collagenous tissues. *J. Biomech. Eng.* 125:280–287.
36. Gasser, T. C., R. W. Ogden, and G. A. Holzapfel. 2006. Hyperelastic modelling of arterial layers with distributed collagen fibre orientations. *J. R. Soc. Interface.* 3:15–35.
37. Kent, J. T. 1982. The Fisher-Bingham distribution on a sphere. *J. R. Stat. Soc., B.* 44:71–80.
38. Nguyen, T. D., and B. L. Boyce. 2011. An inverse finite element method for determining the anisotropic properties of the cornea. *Biomech. Model. Mechanobiol.* 10:323–337.
39. Pijanka, J. K., B. Coudrillier, …, C. Boote. 2012. Quantitative mapping of collagen fiber orientation in non-glaucoma and glaucoma posterior human sclerae. *Invest. Ophthalmol. Vis. Sci.* 53:5258–5270.
40. Coudrillier, B., J. Tian, …, T. D. Nguyen. 2012. Biomechanics of the human posterior sclera: age- and glaucoma-related changes measured using inflation testing. *Invest. Ophthalmol. Vis. Sci.* 53:1714–1728.
41. Coudrillier, B., J. Pijanka, …, T. D. Nguyen. 2015. Collagen structure and mechanical properties of the human sclera: analysis for the effects of age. *J. Biomech. Eng.* 137:041006.

42. Coudrillier, B., J. Pijanka, …, T. D. Nguyen. 2015. Effects of age and diabetes on the scleral stiffness. *J. Biomech. Eng.* 137:071007.

43. Boyce, B. L., J. M. Grazier, …, T. D. Nguyen. 2008. Full-field deformation of bovine cornea under constrained inflation conditions. *Biomaterials.* 29:3896–3904.

44. Gallagher, B., and D. Maurice. 1977. Striations of light scattering in the corneal stroma. *J. Ultrastruct. Res.* 61:100–114.

45. Johnson, K. A., Z. B. Simpson, and T. Blom. 2009. FitSpace Explorer: an algorithm to evaluate multidimensional parameter space in fitting kinetic data. *Anal. Biochem.* 387:30–41.

46. Chang, S.-W., and M. J. Buehler. 2014. Molecular biomechanics of collagen molecules. *Mater. Today.* 17:70–76.

47. Sarkar, S. K., B. Marmer, …, K. C. Neuman. 2012. Single-molecule tracking of collagenase on native type I collagen fibrils reveals degradation mechanism. *Curr. Biol.* 22:1047–1056.